Reconfigurable Topological Phases in Next-Nearest-Neighbor Coupled Resonator Lattices

Daniel Leykam,[1] S. Mittal,[2,3] M. Hafezi,[2,3] and Y. D. Chong[4,5]
[1]Center for Theoretical Physics of Complex Systems, Institute for Basic Science (IBS), Daejeon 34126, Republic of Korea
[2]Joint Quantum Institute, NIST/University of Maryland, College Park, Maryland 20742, USA
[3]Department of Electrical and Computer Engineering and IREAP, University of Maryland, College Park, Maryland 20742, USA
[4]Division of Physics and Applied Physics, School of Physical and Mathematical Sciences, Nanyang Technological University, Singapore 637371, Singapore
[5]Centre for Disruptive Photonic Technologies, Nanyang Technological University, Singapore 637371, Singapore

(Received 13 February 2018; revised manuscript received 25 April 2018; published 9 July 2018)

We present a reconfigurable topological photonic system consisting of a 2D lattice of coupled ring resonators, with two sublattices of site rings coupled by link rings, which can be accurately described by a tight-binding model. Unlike previous coupled-ring topological models, the design is translationally invariant, similar to the Haldane model, and the nontrivial topology is a result of next-nearest couplings with nonzero staggered phases. The system exhibits a topological phase transition between trivial and spin Chern insulator phases when the sublattices are frequency detuned. Such topological phase transitions can be easily induced by thermal or electro-optic modulators, or nonlinear cross phase modulation. We use this lattice to design reconfigurable topological waveguides, with potential applications in on-chip photon routing and switching.

DOI: 10.1103/PhysRevLett.121.023901

Introduction.—Topological photonic systems have attracted significant recent interest due to their potential applications as disorder-robust waveguides and delay lines [1,2]. Topological protection is, however, both a blessing and a curse: steering the flow of light between different channels requires the ability to switch between topological phases by inducing band inversions. Such switching was recently demonstrated using mechanical reconfiguration of microwave photonic crystals and phononic metamaterials [3–6]. It would be interesting to achieve similar functionality in the optical domain, particularly for on-chip applications, using dynamic reconfiguration based on thermal, electro-optic, or nonlinear effects [7–15]. However, existing designs for topological photonic lattices at optical frequencies, such as helical waveguide arrays [16–18] or coupled resonators [19–25] are ill suited because they are based on spatial or temporal modulations and require inhomogeneous tuning to induce phase transitions. For example, the coupled resonator array studied in Ref. [19] uses staggered phase shifts to simulate the integer quantum Hall effect, requiring individual control over these staggered phases.

Here we show that next-nearest neighbor hoppings provide a practical way to achieve reconfigurable topological phases in translationally invariant optical resonator lattices. Importantly, transitions between trivial and nontrivial phases are induced by resonance frequency shifts that are small compared to the rings' free spectral range. We demonstrate the reconfigurability of this system with two examples. In the first, thermal or electro-optic tuning [25,26] of the ring resonances reroutes edge states at an interface between trivial and nontrivial phases. In the second example, a strong pump induces nonlinear cross-phase modulation [27], which then triggers a topological phase transition. The features of our model thus provide a promising route to achieving reconfigurable topological edge modes in optical devices, as well as for studying how optical nonlinearities affect photonic topological edge states.

We consider a 2D bipartite lattice consisting of resonant "site rings" coupled via off-resonant "link rings," with the latter positioned such that they facilitate both nearest-neighbor (NN) and next-nearest neighbor (NNN) hoppings between the sites. The two circulations of light (clockwise or anticlockwise) in each sublattice form a pseudospin degree of freedom; within each spin sector time-reversal ($\mathcal{T}$) symmetry is effectively broken, enabling quantum spin Hall edge states that are immune to backscattering as long as the spins are decoupled [19]. Similar to the Haldane model [28], the simultaneous presence of next-nearest neighbor hoppings and $\mathcal{T}$ breaking gives rise to a phase diagram hosting both trivial (conventional insulator) and nontrivial (spin Chern insulator) phases. By contrast, the nearest neighbor-coupled design introduced by Hafezi *et al.* [19] broke translational symmetry by assigning uniformly increasing phase shifts to the link rings, resulting in a fractal

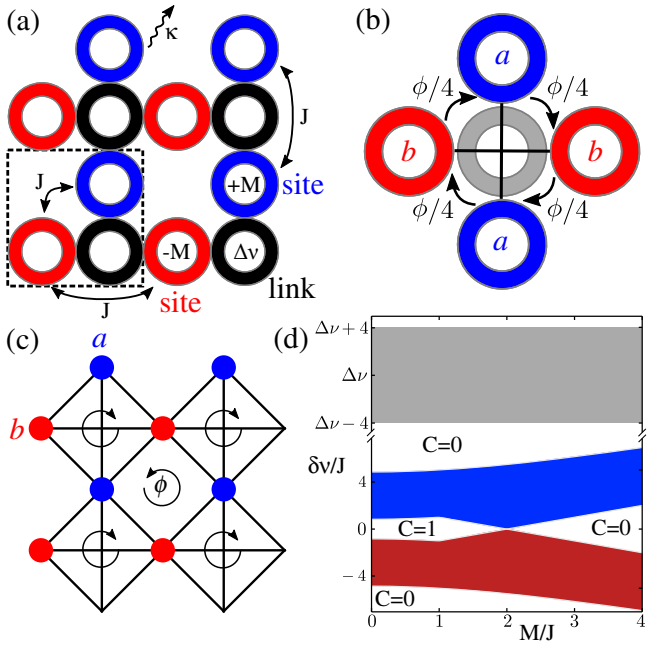

FIG. 1. (a) Square resonator lattice of site rings (blue, red) with relative detuning $\pm M$, coupled with strength J via off-resonant link rings (black) detuned by $\Delta\nu$. All rings have intrinsic loss κ. Dashed line indicates the unit cell. (b) Detailed schematic centered on a single link ring, which mediates both nearest-neighbor and next-nearest-neighbor couplings between site rings, with coupling phases $\pm\phi/4$ and 0, respectively. (c) Tight binding model for the site ring resonances, consisting of a checkerboard lattice with staggered flux $\pm\phi = \pm 2\pi\Delta\nu/\mathrm{FSR}$. (d) Bloch band energies $\delta\nu$ (shaded regions) versus site detuning M, calculated from the tight-binding model for anti-resonant site and link rings ($\phi = \pi$). Red and blue areas indicate the sublattice the modes are localized to in the large M limit. Gap Chern numbers C are indicated and topologically nontrivial link bands occur for $|M| < 2J \csc \phi/2$.

Hofstadter butterfly spectrum [19,21,22,25] and lacking simple topological transitions based on band inversions. On the other hand, band inversions in ring resonator lattices *without* aperiodic elements can also occur in the strong coupling limit described by scattering matrices [29–33], but strong coupling implies low quality factor resonators, which is not useful for the enhancement of nonlinear effects or delay lines.

Figure 1(a) shows a schematic of the 2D lattice. The site rings (shaded red and blue) are positioned on a checkerboard lattice, while the link rings (shaded black) are positioned such that they couple the nearest neighbor site rings (diagonal couplings between red and blue sites) as well as the next-nearest neighbor site rings (horizontal and vertical couplings between red and blue sites, respectively). Furthermore, as shown in Fig. 1(b), the nearest-neighbor couplings between site rings (diagonals) introduce a direction-dependent hopping phase, which arises from the difference in the path lengths traveled in the link rings while hopping in different directions. The NNN hoppings are symmetric and do not carry a direction-dependent phase. In the absence of the NNN couplings, the systems is gapless with a pair of Dirac points; the NNN couplings contribute to opening a nontrivial band gap [28,34]. Note that unlike the system of Ref. [19], the NN hopping phases in our system are periodic, and therefore the lattice is translation invariant.

Tight binding model.—We derive a tight binding model for the lattice by restricting ourselves to one of the two decoupled circulation sectors (anticlockwise site modes) [19], and taking the operating frequency to be close to the resonance frequency of the site rings, which are detuned from the link rings by $\Delta\nu$. The effective intersite coupling can be derived by considering two site rings connected by a link ring, as in Ref. [21], and depends on the parameter

$$\phi = 2\pi\Delta\nu/\mathrm{FSR}, \tag{1}$$

where $\mathrm{FSR} \approx 10^3$ GHz is the rings' free spectral range [21] (we assume the site and link rings have similar dimensions).

We assume that the rings are weakly coupled high quality factor resonators, so that $J \ll (\Delta\nu, \mathrm{FSR})$, where J is the intersite coupling strength for antiresonant sites and links (i.e., when $\phi = \pi$). Moreover, we apply a small detuning M between the two site ring sublattices; inversion symmetry is broken for $M \neq 0$, which will be the mechanism for inducing a topological transition. Using the weak-coupling approximation to eliminate the link ring amplitudes as modal variables, we derive the tight binding Hamiltonian $\hat{H}$ [35]:

$$\begin{aligned}
\hat{H} &= \sum_{x,y} (\hat{H}_a + \hat{H}_b + \hat{H}_{ab} + \hat{H}_{ab}^\dagger), \\
\hat{H}_a &= \hat{a}_{x,y}^\dagger \left(\left(2J \cot\frac{\phi}{2} + M \right) \hat{a}_{x,y} + J \csc\frac{\phi}{2} \sum_{\pm} \hat{a}_{x,y\pm 1} \right), \\
\hat{H}_b &= \hat{b}_{x,y}^\dagger \left(\left(2J \cot\frac{\phi}{2} - M \right) \hat{b}_{x,y} + J \csc\frac{\phi}{2} \sum_{\pm} \hat{b}_{x\pm 1,y} \right), \\
\hat{H}_{ab} &= J e^{i\phi/4} \csc\frac{\phi}{2} \\
&\quad \times [\hat{a}_{x,y}^\dagger (\hat{b}_{x,y} + \hat{b}_{x+1,y+1}) + \hat{b}_{x,y}^\dagger (\hat{a}_{x-1,y} + \hat{a}_{x,y-1})].
\end{aligned} \tag{2}$$

Here, $\hat{a}^\dagger$ and $\hat{b}^\dagger$ are creation operators for the a and b sublattices, respectively, (x, y) are integers indexing the lattice sites, the effective coupling is $J \csc(\phi/2)$, and $J \cot(\phi/2)$ is a coupling-induced frequency shift.

Note that the NN and NNN coupling strengths are equal in magnitude. By contrast, in the topological photonic lattices studied in Refs. [16–22,25], NNN couplings are either absent or negligible compared to NN couplings. In momentum space, the Schrödinger equation governing the evolution of the field amplitudes $\psi = (\psi^{(a)}, \psi^{(b)})$ can be compactly written as

$$
\begin{aligned}
i\partial_t\psi &= [\delta\nu - \hat{H}(k_x, k_y)]\psi, \\
\hat{H} &= J\csc(\phi/2)\begin{pmatrix} d_0 + d_z & d_x - id_y \\ d_x + id_y & d_0 - d_z \end{pmatrix}, \\
d_0 &= 2\cos(\phi/2) + \cos k_x + \cos k_y, \\
d_x &= 4\cos(\phi/4)\cos(k_x/2)\cos(k_y/2), \\
d_y &= -4\sin(\phi/4)\sin(k_x/2)\sin(k_y/2), \\
d_z &= \frac{M}{J}\sin(\phi/2) - \cos k_x + \cos k_y. \qquad (3)
\end{aligned}
$$

Here, $\delta\nu \equiv \nu - \nu_0 - i\kappa$, where ν is the operating frequency, ν_0 is the site resonance frequency, and $\kappa \ll \mathrm{FSR}$ is the loss rate in each ring.

If the two types of site rings are identical ($M = 0$), the two bands of $\hat{H}$ have Chern numbers $C = \pm 1$, with a gap of size $\Delta = 2J\sec^2(\phi/8)/[1 + \tan(\phi/8)] \sim 2J$, containing topologically protected edge states. As shown in Fig. 1(d), we can induce a topological transition into a trivial phase (where the bands' Chern numbers are zero) by varying M. The transition point lies at $M = 2J\csc(\phi/2) \sim J \ll (\Delta\nu, \mathrm{FSR})$. This implies that the transition can be realized via weak physical effects, affecting either the site rings (varying M) or the link rings (varying $\Delta\nu$ and hence M_c). At the transition point, the band structure contains a single Dirac point at either $(k_x, k_y) = (0, \pi)$ (if $M > 0$) or $(\pi, 0)$ (if $M < 0$).

We have tested the validity of the tight binding model by comparing the bulk spectrum of $\hat{H}$ to the transfer matrix description. The spectra are in good agreement, with band edge frequencies accurate to within 10% for the moderate coupling strengths typically used in experiment ($J/\mathrm{FSR} \sim 0.01$). For large couplings ($J/\mathrm{FSR} \approx 0.06$ for $\phi = \pi$), the two-band tight binding approximation breaks down, in which case either a three-band tight binding model or the full transfer matrix formalism must be used. Details are given in the Supplemental Material [35].

Having derived an accurate tight-binding Hamiltonian, we can use it in schemes for routing topological edge states [3–6], manipulating topological edge states with optical nonlinearities [9,10,13,14], and other interesting possibilities. Two examples are presented below.

Reconfigurable domain wall.—The resonance frequencies of optical ring resonators can be actively controlled using on-chip thermal [25] or electro-optic modulators [26]. By using such methods to adjust the detuning M between vertical and horizontal site rings, we can selectively induce a topological transition in part of a lattice (without any spectral shift), producing domains with topologically distinct gaps at the same frequency. This would allow us to realize a reconfigurable topological waveguide [3–6].

Figure 2 shows an example of such a scheme. The lattice contains two domains, with $M = M_1$ on the left and $M = M_2$ on the right, with all other lattice parameters the same. By controlling these detunings, we can define a domain with a nontrivial gap (with $M = J$) and a domain

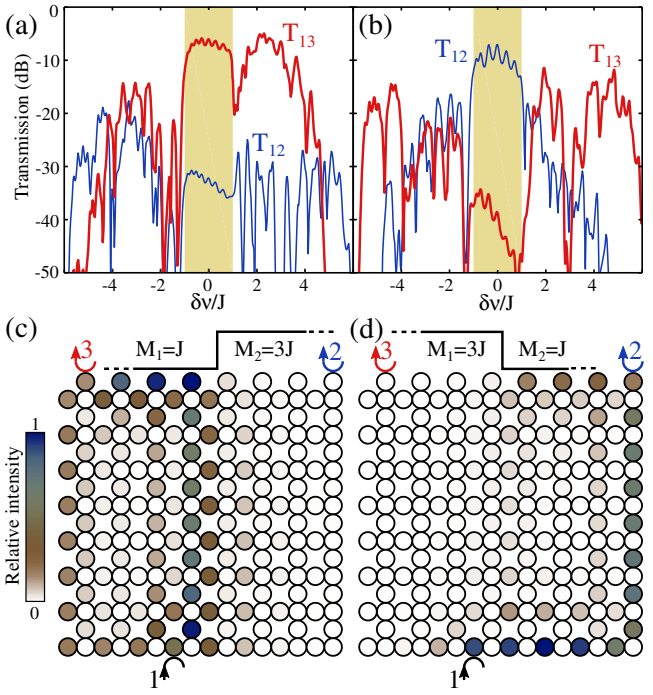

FIG. 2. Reconfigurable topological waveguide functionality enabled by active control of site ring detunings. The lattice contains 8×8 unit cells, with two domains where $M = M_1$ and $M = M_2$, respectively, with $\kappa = 0.05J$ and $\phi = \pi$ (i.e., site and link rings detuned by FSR/2) throughout. The couplings at the inputs and outputs are $\kappa_{\mathrm{ex}} = 2J$. (a) Transmission curves for $M_1 = J$ and $M_2 = 3J$; the positions of the input port (1) and output ports (2,3) are shown in (c), and the band gaps are shaded in yellow. (b) Transmission curves for $M_1 = 3J$ and $M_2 = J$. (c)–(d) Intensity profiles at the midgap frequency $\delta\nu = 0$.

with a trivial gap (with $M = 3J$). In practice, this can be accomplished by fabricating an array with uniform site offsets $\nu_a = J$ and $\nu_b = -3J$, and then in each domain detuning either ν_a or ν_b by $2J$. In other words, we need only a binary shift of the site resonances (0 or $2J$), rather than the inhomogeneous shifts required in Ref. [21], or the much stronger shifts ($\approx$FSR/2) in the strongly coupled ring lattice discussed in Ref. [32].

As shown in Figs. 2(c)–2(d), we define an input port 1 that couples to a single site ring, and output ports 2 and 3 on opposite corners of the lattice. The input and output couplings are described by

$$
i\partial_t\psi_{\mathrm{in}}^{(b)} = (\delta\nu - i\kappa_{\mathrm{ex}} - \hat{H})\psi_{\mathrm{in}}^{(b)} + i\sqrt{2\kappa_{\mathrm{ex}}}\varepsilon_{\mathrm{in}}, \qquad (4)
$$

$$
i\partial_t\psi_{\mathrm{out,j}}^{(a)} = (\delta\nu - i\kappa_{\mathrm{ex}} - \hat{H})\psi_{\mathrm{out,j}}^{(a)}, \qquad (5)
$$

where κ_{ex} is the input-output coupling rate, $\psi_{\mathrm{in}}^{(b)}$ denotes the input site, and $\psi_{\mathrm{out},j}^{(a)}$ ($j = 1, 2$) are the output sites. From these, we can compute the steady-state transmittances $T_{1j} = 2\kappa_{\mathrm{ex}}|\psi_{\mathrm{out,j}}^{(a)}|^2/\varepsilon_{\mathrm{in}}^2$.

Figure 2 plots the transmission spectra and midgap intensity profiles for the two choices of interface orientation, with $\kappa = 0.05J$, $\kappa_{ex} = 2J$, and lattice size $N = 8$ [21]. Broad transmission maxima limited only by the intrinsic absorption κ occur in the band gap of the array, mediated by topological edge modes, with the transmission to the alternate output port suppressed by over 30 dB. In the Supplemental Material, we show that this transmission is robust against spin-conserving disorder [35], which is the most significant source of backscattering in typical coupled resonator optical waveguides [21,22]. Moreover, the large topological band gap can approach the free spectral range in experimentally realistic settings. For example, in Ref. [25] the thermo-optic modulators induced shifts of up to 0.3 FSR = 300 GHz. Employing a similar shift in this design allows for reconfigurable topologically protected pass bands of width 200–300 GHz, which is promising for wavelength-division multiplexing applications.

Pump-induced topological transition.—The tight-binding model can also be used to design a device exhibiting nonlinearity-controlled topological transport. To demonstrate this, we fix the detuning M and use cross phase modulation (acting on ϕ) to tune between trivial and nontrivial phases. A strong pump, resonant with the link rings, shifts their resonance frequency such that [36]

$$\phi = \phi_0 - 4\pi\nu_{\mathrm{NL}}|\psi^{(s)}_{x,y}|^2/\mathrm{FSR}, \tag{6}$$

where ϕ_0 is the coupling parameter in the absence of the pump, ν_{NL} is the effective Kerr coefficient, and the pump beam profile $\psi^{(s)}_{x,y}$ is governed by a square lattice tight binding model for the link rings [35]. Assuming a uniform pump intensity $|\psi^{(s)}_{x,y}|^2 = I$, one can calculate the band structure and Chern numbers for a weak probe beam using the linear tight binding model Eq. (3) with effective coupling parameter Eq. (6); a phase transition between trivial and nontrivial phases occurs at the critical pump intensity $I = \mathrm{FSR}[\phi_0 - \sin^{-1}(2J/M)]/4\pi\nu_{\mathrm{NL}}$.

As an example, we consider a homogeneous lattice with $M = -2.4J$ and $\phi_0 = 0.65\pi$ (in the trivial phase). We couple a monochromatic pump at frequency $\nu - \nu_L = 4.6J$ into an edge link ring with strength $\kappa_{ex} = J/2$, solving its nonlinear propagation equation in the time domain [35] and including moderate two photon absorption $\kappa_{\mathrm{NL}} = 0.1\nu_{\mathrm{NL}}$ representative of the resonators used in Ref. [21]. At a critical power the pump converges to the stable steady state shown in Figs. 3(a), 3(b), resulting in an average shift to the coupling parameter of $\phi_0 - \phi \approx 0.1\pi$, which is sufficient to induce a transition to the Chern insulator phase for the probe field.

In Fig. 3(c), we compute the transmission spectrum of a weak probe beam tuned to the site bands. Without the pump, the site bands are topologically trivial and the band gap forms a deep transmission minimum. When the pump is applied, the midgap transmission is increased by

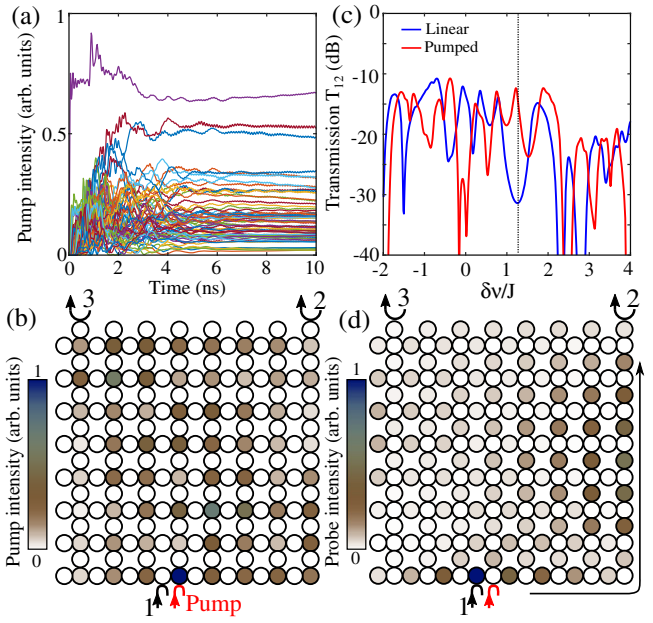

FIG. 3. Nonlinearity-induced topological transition. (a),(b) Solution of the nonlinear scattering equations for a pump beam at $\nu - \nu_L = 4.6J$. (a) Dynamics of link ring intensities, illustrating relaxation to a stable steady state within 5 ns. The different colors denote different link rings. (b) Resulting pump intensity profile over the 8×8 lattice inducing a Chern insulator phase at the site resonance. Red arrow indicates the pump input position relative to the probe ports (1,2,3). (c) Transmission spectrum at the site resonance without (blue) and with (red) the pump beam. (d) Midgap probe profile when pump is applied [frequency indicated by dashed line in (c)].

≈ 20 dB due to the formation of an additional resonance associated with a topological edge state. Figure 3(d) plots the probe's intensity profile, which is directed along the edge and to output port 2 despite the disorder induced by the inhomogeneity of the pump.

It is interesting to note that the large increase in the transmission of Fig. 3(c) is not easily achievable using the previously studied self-focusing nonlinearity of a bright probe beam. First, two-photon absorption will inevitably result in increased attenuation of a high power probe [27]. Furthermore, modulational instability may break up the topological edge states [8,11,12]. On the other hand, using this pump-probe scheme, the nonlinearity is confined to the link rings, where the probe photons spend relatively little time. Consequently, parametric mixing processes between pump and probe are suppressed, and to a good approximation the probe beam dynamics remain governed by a linear Hamiltonian, and the well-established robustness of linear topological edge states holds. For these reasons, pump-induced cross phase modulation is a highly promising alternative for ultrafast and robust nonlinear switching of topological edge states.

Outlook.—We have designed a lattice of coupled ring resonators that serves as a promising setting for electro-optic

or nonlinearly-reconfigurable topological waveguiding at optical frequencies. The distinguishing feature of this scheme is the use of a bipartite lattice; for a given circulation, the corresponding tight-binding model is $\mathcal{T}$ broken and has both nearest-neighbor and next-nearest-neighbor couplings, which are of equal magnitude. The phase diagram contains both conventional insulator and Chern insulator phases, and the lattice can be tuned between them via experimentally accessible parameters.

Note also that previous methods relying on aperiodic couplings [19,21] or dynamic modulation [20,23,24] introduce an additional length or energy scale to the system that constrains the bandwidth of the topological phase. For example, dynamic modulation requires the interresonator coupling to be much weaker than the modulation frequency; Ref. [24] estimated a maximum practical band gap of 33 GHz using terahertz Kerr modulation. Such constraints are bypassed in next-nearest-neighbor coupled models, enabling broadband operation approaching the rings' free spectral range.

We demonstrated switching of topological edge states based on static detuning of the link resonators or nonlinear cross phase modulation of the site resonators. The latter requires nonlinear resonance shifts of approximately 50 GHz (5% of the free spectral range), which is well within reach of current silicon photonics technology. Our scheme can be readily generalized other classes of simple lattices, such as hexagonal or honeycomb lattices, where the larger number of coupled neighbors will result in Chern insulators with longer range coupling, broader bandwidths, and multiple band gaps.

This research was supported by the Institute for Basic Science in Korea (IBS-R024-Y1), the Singapore MOE Academic Research Fund Tier 2 (MOE2015-T2-2-008), the Singapore MOE Academic Research Fund Tier 3 (MOE2016-T3-1-006), AFOSR MURI Grant No. FA95501610323, ONR, the Sloan Foundation, and the Physics Frontier Center at the Joint Quantum Institute.

[1] L. Lu, J. D. Joannopoulos, and M. Soljačić, Topological photonics, Nat. Photonics **8**, 821 (2014).
[2] Y. Wu, C. Li, X. Hu, Y. Ao, Y. Zhao, and Q. Gong, Applications of topological photonics in integrated photonic devices, Adv. Opt. Mater. **5**, 1700357 (2017).
[3] T. Ma, A. B. Khanikaev, S. H. Mousavi, and G. Shvets, Guiding Electromagnetic Waves Around Sharp Corners: Topologically Protected Photonic Transport in Metawaveguides, Phys. Rev. Lett. **114**, 127401 (2015).
[4] X. Cheng, C. Jouvaud, X. Ni, S. H. Mousavi, A. Z. Genack, and A. B. Khanikaev, Robust reconfigurable electromagnetic pathways within a photonic topological insulator, Nat. Mater. **15**, 542 (2016).
[5] M. Goryachev and M. E. Tobar, Reconfigurable Microwave Photonic Topological Insulator, Phys. Rev. Applied **6**, 064006 (2016).
[6] R. Süsstrunk, P. Zimmermann, and S. D. Huber, Switchable topological phonon channels, New J. Phys. **19**, 015013 (2017).
[7] Y. Lumer, Y. Plotnik, M. C. Rechtsman, and M. Segev, Self-Localized States in Photonic Topological Insulators, Phys. Rev. Lett. **111**, 243905 (2013).
[8] M. J. Ablowitz, C. W. Curtis, and Y.-P. Ma, Linear and nonlinear traveling edge waves in optical honeycomb lattices, Phys. Rev. A **90**, 023813 (2014).
[9] Y. Hadad, A. B. Khanikaev, and A. Alu, Self-induced topological transitions and edge states supported by nonlinear staggered potentials, Phys. Rev. B **93**, 155112 (2016).
[10] D. Leykam and Y. D. Chong, Edge Solitons in Nonlinear-Photonic Topological Insulators, Phys. Rev. Lett. **117**, 143901 (2016).
[11] Y. Lumer, M. C. Rechtsman, Y. Plotnik, and M. Segev, Instability of bosonic topological edge states in the presence of interactions, Phys. Rev. A **94**, 021801(R) (2016).
[12] Y. V. Kartashov and D. Skyrabin, Modulational instability and solitary waves in polariton topological insulators, Optica **3**, 1228 (2016).
[13] Y. Hadad, V. Vitelli, and A. Alu, Solitons and propagating domain walls in topological resonator arrays, ACS Photonics **4**, 1974 (2017).
[14] X. Zhou, Y. Wang, D. Leykam, and Y. D. Chong, Optical isolation with nonlinear topological photonics, New J. Phys. **19**, 095002 (2017).
[15] M. I. Shalaev, S. Desnavi, W. Walasik, and N. M. Litchinitser, Reconfigurable topological photonic crystal, New J. Phys. **20**, 023040 (2018).
[16] M. C. Rechtsman, J. M. Zeuner, Y. Plotnik, Y. Lumer, D. Podolsky, F. Dreisow, S. Nolte, M. Segev, and A. Szameit, Photonic Floquet topological insulators, Nature (London) **496**, 196 (2013).
[17] D. Leykam, M. C. Rechtsman, and Y. D. Chong, Anomalous Topological Phases and Unpaired Dirac Cones in Photonic Floquet Topological Insulators, Phys. Rev. Lett. **117**, 013902 (2016).
[18] J. Noh, S. Huang, D. Leykam, Y. D. Chong, K. Chen, and M. C. Rechtsman, Experimental observation of optical Weyl points and Fermi arc-like surface states, Nat. Phys. **13**, 611 (2017).
[19] M. Hafezi, E. A. Demler, M. D. Lukin, and J. M. Taylor, Robust optical delay lines with topological protection, Nat. Phys. **7**, 907 (2011).
[20] K. Fang, Z. Yu, and S. Fan, Realizing effective magnetic field for photons by controlling the phase of dynamic modulation, Nat. Photonics **6**, 782 (2012).
[21] M. Hafezi, S. Mittal, J. Fan, A. Migdall, and J. M. Taylor, Imaging topological edge states in silicon photonics, Nat. Photonics **7**, 1001 (2013).
[22] S. Mittal, J. Fan, S. Faez, A. Migdall, J. M. Taylor, and M. Hafezi, Topologically Robust Transport of Photons in a Synthetic Gauge Field, Phys. Rev. Lett. **113**, 087403 (2014).
[23] V. Peano, C. Brendel, M. Schmidt, and F. Marquardt, Topological Phases of Sound and Light, Phys. Rev. X **5**, 031011 (2015).
[24] M. Minkov and V. Savona, Haldane quantum Hall effect for light in a dynamically modulated array of resonators, Optica **3**, 200 (2016).

[25] S. Mittal, S. Ganeshan, J. Fan, A. Vaezi, and M. Hafezi, Measurement of topological invariants in a 2D photonic system, Nat. Photonics **10**, 180 (2016).

[26] C. Qiu, W. Gao, R. Vajtai, P. M. Ajayan, J. Kono, and Q. Xu, Efficient modulation of 1.55 μm radiation with gated graphene on a silicon microring resonator, Nano Lett. **14**, 6811 (2014).

[27] J. Leuthold, C. Koos, and W. Freude, Nonlinear silicon photonics, Nat. Photonics **4**, 535 (2010).

[28] F. D. M. Haldane, Model for a Quantum Hall Effect Without Landau Levels: Condensed-Matter Realization of the "Parity Anomaly", Phys. Rev. Lett. **61**, 2015 (1988).

[29] G. Q. Liang and Y. D. Chong, Optical Resonator Analog of a Two-Dimensional Topological Insulator, Phys. Rev. Lett. **110**, 203904 (2013).

[30] M. Pasek and Y. D. Chong, Network models of photonic Floquet topological insulators, Phys. Rev. B **89**, 075113 (2014).

[31] W. Hu, J. C. Pillay, K. Wu, M. Pasek, P. P. Shum, and Y. D. Chong, Measurement of a Topological Edge Invariant in a Microwave Network, Phys. Rev. X **5**, 011012 (2015).

[32] F. Gao, Z. Gao, X. Shi, Z. Yang, X. Lin, H. Xu, J. D. Joannopoulos, M. Soljacic, H. Chen, L. Lu, Y. Chong, and B. Zhang, Probing topological protection using a designer surface plasmon structure, Nat. Commun. **7**, 11619 (2016).

[33] T. Shi, H. J. Kimble, and J. I. Cirac, Topological phenomena in classical optical networks, Proc. Natl. Acad. Sci. U.S.A. **114**, E8967 (2017).

[34] W. Beugeling, J. C. Everts, and C. M. Smith, Topological phase transitions driven by next-nearest-neighbor hopping in two-dimensional lattices, Phys. Rev. B **86**, 195129 (2012).

[35] See Supplemental Material at http://link.aps.org/supplemental/10.1103/PhysRevLett.121.023901 for the derivation of the tight binding model and simulations showing disorder-robust transmission.

[36] G. Agarwal, *Nonlinear Fiber Optics* (Academic, New York, 2007).